Iron and Steelmaker, Vol. 24, No. 8, Iron and Steel Society, Warrendale, PA, 1997, pp. 31-38.

Model of Inclusion Removal during RH Degassing of Steel

Yuji Miki+, Brian G. Thomas*
Alex Denissov*, Yasushi Shimada+
+Kawasaki Steel Corp.
1 Kawasaki-cho Cyuo-ku Chiba-shi, 260 Japan
*University of Illinois at Urbana-Champaign
1206 W. Green St. Urbana, IL 61801

ABSTRACT

Mathematical models are applied to simulate multiphase, turbulent fluid flow in a RH degassing vessel using FLUENT, including the motion of molten steel, injected argon gas, inclusion particles, and the top free surface. Predicted inclusion removal rates are validated with measurements based on samples collected from operating degassers. The results quantify the important role of argon gas bubbles on the inclusion removal mechanism.

1. INTRODUCTION

The importance of molten steel cleanliness is increasing with the demand of high quality steel. A RH degasser plays an important role not only for decarburization but also for inclusion removal. However, inclusion removal involves complex phenomena, such as, inclusion coagulation by collision, inclusion flotation, attachment to bubbles and the flow pattern, which have not been clarified perfectly.

Concerning inclusion collision, Torssell et.al.[1] calculated the change of oxygen content using the Stokes' collision model. Also, K. Nakanishi and J. Szekely[2] calculated inclusion size distribution assuming that inclusions were collided in turbulence eddies by using the Saffman and Turner's theory[3] and inclusions with radius more than 16 µm disappear instantly.

The collision of particles in turbulent flow has been studied in other engineering fields. K. Higashitani et al.[4] studied collision of latex particles in water and calculated the size distribution. They used a model with the effect of viscous fluid and interaction between particles and got good agreement with observed.

Concerning inclusion flotation and flow pattern, inclusion motion in a tundish and a mold has been calculated and good agreement with water model experiments were obtained[5].

Attachment to bubbles is also discussed[6]. However, the complete mechanisms of inclusion removal in actual processes have not been clarified.

In this work, a numerical model of inclusion collision and removal in a RH degasser is developed and compared with measurements of inclusion size distributions based on a new technology involving acid extraction and laser diffraction[7]. The findings are used to understand the mechanism of inclusion removal and practical implications.

2. METHOD OF NUMERICAL MODEL.

In this model, inclusion coagulation, inclusion removal by flotation, fluid flow pattern, and inclusion entrapment to argon bubbles are calculated to predict the change of inclusion size distribution during RH degassing. Fig.1 shows the calculation steps.

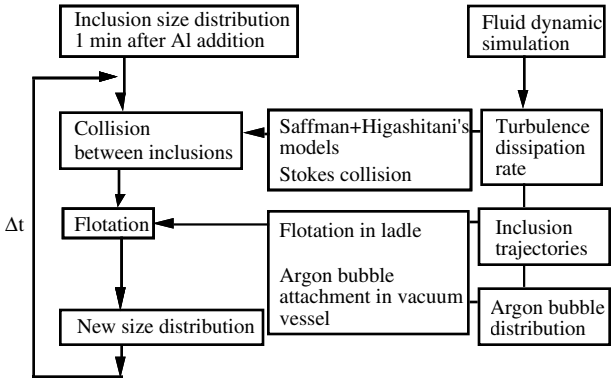

Fig.1 Model flow chart.

2.1. Evolution of Inclusion Size Distribution.

The inclusion size distribution is governed by conservation of mass within each size range and time step. Inclusion radii were discretized into 0.05 µm intervals starting from 0 - 0.05 µm with average radius r_k in the k-th size range. The rate of change of the number of inclusions in each size range, $f(r_k)$, is calculated by

$$\frac{df(r_k)}{dt} = \frac{1}{2}\sum_{i=1}^{i=k-1} f(r_i) f(r_{k-i}) W(i,k-i) - \sum_{i=1}^{i\max} f(r_i) f(r_k) W(i,k) - S \qquad (1)$$

under the condition, $r_{k-i}^3 = r_k^3 - r_i^3$ (2)

The 3 terms in the right-hand side of Eq.(1) represent mass generation (from the agglomeration of smaller particles, i and k-i), disappearance (from agglomeration into larger particles due to collision with every possible

size range and inclusions of each inclusion particle size range, r_k) and flotation removal. $W(r_i, r_{k-i})$ is the rate of collision between inclusions of radius r_i and r_{k-i} inclusion and S is the rate of inclusion removal by flotation.
Inclusion collisions occur mainly in turbulent eddies and are proportional to the turbulence dissipation rate and the difference in Stokes flotation rate between two particles.

$$W = W_t + W_s \qquad (3)$$

Where, W_t : collision rate of inclusions in turbulence eddies, W_s : rate of Stokes collision.

Functions in these equations depend on the submodels of inclusion collision, inclusion flotation and argon bubble entrapment. Each submodel is discussed in the following sections.

2.2. Inclusion Collision Model.

The collision rate in turbulence eddies is calculated using the Saffman and Turner model, Higashitani's theory and Stokes collision theory.
The collision rate between two inclusions of size ranges, r_i, r_j , is expressed by Saffman and Turner[3].

$$W_t(r_i, r_j) = 1.3\alpha(r_i + r_j)^3 \left(\frac{\varepsilon}{\nu}\right)^{0.5} \qquad (4)$$

Where, r_i, r_j : inclusion radius, ε : turbulence dissipation rate, ν : kinematic viscosity.

The empirical coefficient of collision, α was introduced by K. Nakanishi and J. Szekely[2]. α was estimated to be 0.27-0.63 by comparing the calculated oxygen contents and the measured ones.

K. Higashitani et al.[4] suggested the following equations to find α. In their model, increased fluid viscosity reduces the collision rate and interaction between particles is considered.

$$\alpha = C_1 \log N + C_2 \qquad (5.1)$$

$$N = \frac{6\pi\mu(r_i + r_j)^3 \sqrt{4\varepsilon/15\pi\nu}}{A} \qquad (5.2)$$

Where, μ : viscosity of molten steel, A : Hamaker constant, N : non-dimensional number (ratio between the viscous force and van der Waals force), ε : turbulence dissipation rate, ν : kinematic viscosity, C_1, C_2 : empirical constants.

The difference of flotation velocity between large and small inclusions also promotes collision. The Stokes collision rate, W_s, is presented by Eq.(6)[1].

$$W_s = \frac{2\pi\Delta\rho g}{9\mu}(r_i + r_j)^3 \,|\, r_i - r_j \,| \qquad (6)$$

Where, r_i, r_j : radius of inclusions, Δρ : the difference of density between inclusions and molten steel, μ : viscosity of molten steel.

2.3. Stokes Flotation.

The rate of inclusion removal by flotation, S, is calculated using the following equation assuming Stokes' terminal velocity and homogeneous inclusion distribution.

$$S = f(r) v dt / L \qquad (7.1)$$

$$v = \frac{2g}{9\mu}\Delta\rho r^2 \qquad (7.2)$$

Where, v : terminal velocity of inclusions in molten steel, g : gravity acceleration, μ : viscosity of molten steel, r : radius of inclusions, L : depth of the molten steel in a vessel.

The rate of flotation varies with the instantaneous inclusion size distribution.

2.4. Fluid Flow Simulation.

To determine the argon bubble distribution and the turbulence dissipation rate, multiphase fluid flow in a RH degasser vessel is simulated using the VOF (Volume-fraction of Fluid) model in the fluid-dynamics code, FLUENT[8].

For simulation in the vacuum vessel, the VOF model is employed to calculate the effect of the argon phase. The interface between the steel and gas phases is tracked by a continuity equation for the volume fraction, f. For each phase, this equation has the form.

$$\frac{\partial f_k}{\partial t} + u_i \frac{\partial f_k}{\partial x_i} = 0 \qquad (8)$$

Where, k : steel, gas
A single momentum equation is solved throughout the domain, and the resulting velocity field is shared among the phases. The momentum equation is dependent on f through the average density, ρ and average turbulent viscosity, μ, which depends on the turbulence parameters k and ε.

$$\frac{\partial}{\partial t}\rho u_j + \frac{\partial}{\partial x_i}\rho u_i u_j = -\frac{\partial P}{\partial x_i} + \frac{\partial}{\partial x_i}\mu\left(\frac{\partial u_i}{\partial x_j} + \frac{\partial u_j}{\partial x_i}\right) + \rho g_j + F_j \qquad (9)$$

$$\rho = f_{steel}\rho_{steel} + f_{gas}\rho_{gas} \qquad (10.1)$$

$$\mu_{eff} = \mu_0 + \mu_t = \mu_0 + \rho C_\mu \frac{k^2}{\varepsilon} \qquad (10.2)$$

$$\mu_0 = f_{steel}\mu_{steel} + f_{gas}\mu_{gas} \qquad (10.3)$$

Where, μ_0 : laminar viscosity, C_μ : empirical constant, 0.09.

2.5. Effect of Argon Bubbles.

The rate of attachment of inclusions to an argon bubble is calculated assuming that the inclusion centerlines flow along streamlines and attaches on the bubble if that streamline comes closer to the bubble than the inclusion radius. The streamline around a bubble is calculated by Eq.(11)[9] assuming potential flow.

$$\varphi = \frac{1}{2} U \sin^2\theta (R^2 - \frac{a^3}{R}) \qquad (11)$$

Where, φ : stream function, U : bulk velocity, a : radius of a bubble.
This equation is used to back calculate the critical entrapment distance, b. Calculated streamlines around a 5 mm diameter argon bubble are shown in Fig.2.

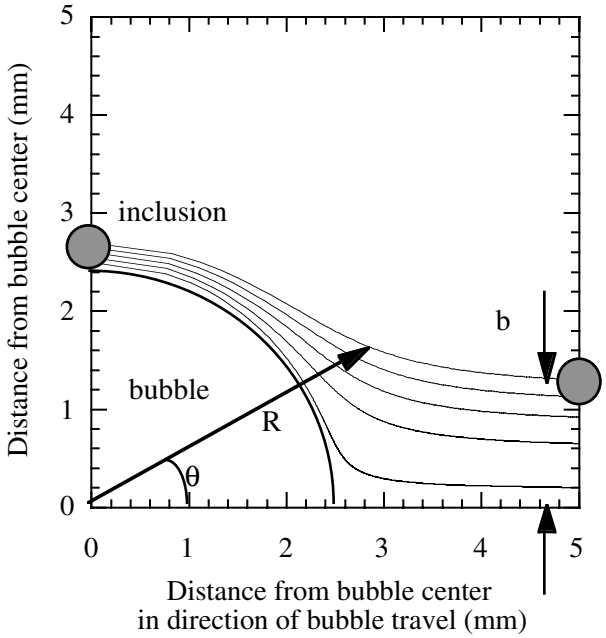

Fig.2 Streamlines around a bubble.

The difference of the velocity between steel and bubbles, v_b is estimated as 0.3 m/sec[10]. When the inclusion is in the volume of $v_b\, b^2\pi$, the inclusion attaches to the bubble within a second. Assuming inclusions are distributed homogeneously, the rate of inclusion entrapment, S_b, is expressed by Eq.(12).

$$S_b = N_b v_b b^2 \pi / V \qquad (12)$$

Where, N_b : number of bubbles, v_b : velocity difference between bubble and steel, V : volume of whole molten steel.

This equation expresses the rate of attachment between bubbles and inclusions. To capture the inclusions, sliding time is necessary. Wang et al.[6] suggested that the probability of this adhesion after the attachment is very low for large inclusions. In this model, the adhesion probability is assumed to be 3 %.

Assuming that all argon bubbles have 5 mm diameter, the number of argon bubbles concentrated in the up-leg is estimated as $3.6*10^6$ based on the multiphase fluid flow model results.

Inclusions attached to argon bubbles in this manner are assumed to be removed in the slag layer above the ladle or the top free surface of the RH degasser.

2.6. Cluster Radius and Density.

The radius of a Al_2O_3 cluster for collision calculations is considered to be that of the circumambient sphere. Tozawa et al.[11] used the fractal theory to relate measured radii of clusters and number of particles composing a cluster.

$$N = d^{1.8} D^{1.8} \qquad (13)$$

Where, N : number of particles in a cluster, d : diameter of a particle, D : diameter of a cluster.

Using Eq.(13), the radius of a circumambient sphere of a cluster, R_c is calculated from the measured radius of a equivalent sphere, R_m in Eq.(14).

$$R_c = (d/2)^{1.8} R_m^{5/3} \qquad (14)$$

The concept of radius of a circumambient sphere and radius of a solid sphere is shown in Fig.3.

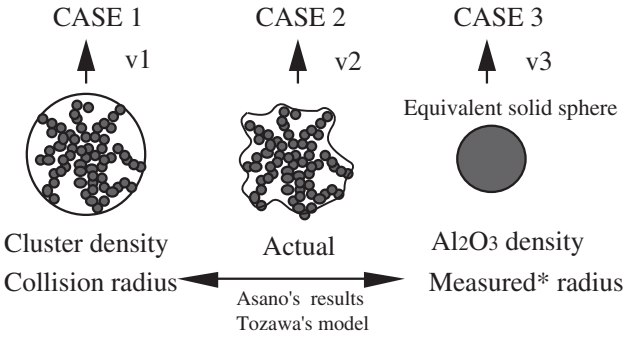

Fig.3 Concept of inclusion radius and density. (* Sphere with the same mass as measured particle from laser diffraction scattering)

The diameter of particles in a cluster, d, is about 1.5 μm based on the inclusion measurements.

Density of a cluster is estimated as a function of volume fraction of Al_2O_3 in the cluster.

$$\rho_{cluster} = (1-\beta)\rho_{Fe} + \beta\rho_{Al_2O_3} \qquad (15)$$

Where, $\rho_{cluster}$: density of cluster, $\rho_{Al_2O_3}$: density of Al_2O_3, ρ_{Fe} : density of steel, β : volume fraction of Al_2O_3 in a cluster.

Asano et al.[12] measured the volume fraction of Al_2O_3 in clusters and concluded the fraction is about 0.03. From Eq.(15), when β is equal to 0.03 for large clusters, the density of inclusions is almost same as that of steel. That is, there is little driving force for large clusters to float.

In Eq.(15), the entire cluster including steel spaces is assumed to move at uniform velocity as shown in CASE 1 in Fig.3. The flotation velocity of an equivalent mass sphere made of Al_2O_3, CASE 3 of Fig.3, is larger than that of the actual cluster. The flotation velocity of a CASE 1 cluster (with β=0.03) is believed to be smaller than that of the actual cluster, CASE 2. Therefore, inclusions are considered to move at a velocity between CASE 1 and CASE 3.

2.7. Inclusion Trajectories.

Inclusion trajectories are calculated using the Langrangian particle tracking method which solves a transport equation for each inclusion as it travels through the molten steel. The force balance on the inclusion includes buoyancy and drag force relative to the steel.

Also, a discrete random walk model is applied for calculations of inclusion trajectories. In this model, a random velocity component is added to the calculated particle velocity to simulate its interaction with a succession of discrete stylized fluid phase turbulent eddies. This random component is proportional to the turbulent energy level, k.

2.8. Conditions and Numerical Error.

Table 1 shows the molten steel properties and operating conditions assumed in modeling of a RH degasser.

Table 1 Calculation and operating conditions.

μ	0.0057 kg/ms
ρ_{Fe}	7000 kg/m^3
ρ_{Al2O3}	3500 kg/m^3
Hamaker constant A	0.45 10^{-20} J [13]
Total molten steel in RH	250 ton
Circulation rate	200 ton/min
Argon flow rate	2000 l/min (STP)

The error in the balance on total mass, M, shown in Eq.(16) was always less than 5%.

M (measured initial inclusion) = M(inclusion floated out) + M(inclusion more than 35 μm) + M(inclusion in molten steel) (16)

The inclusion size distribution when the maximum radius is 35 μm is not different from that when the maximum radius is 50 μm since the number of inclusions larger than 35 μm is very small. Therefore, the maximum radius is assumed to be 35 μm to save calculation time.

3. MEASUREMENT OF INCLUSION SIZE DISTRIBUTION.

Samples were taken in a ladle at 1 min, 7 min and 15 min after aluminum addition during RH degassing. Inclusions were extracted by an acid technique and inclusions size distributions were measured by the laser diffraction scattering method[7]. The radius is measured as the equivalent solid sphere. These measured size distributions are converted to equivalent cluster size distributions for use in the subsequent models using Eq.(14).

Photo.1 shows a typical SEM image of the extracted inclusions. At 1 min after aluminum addition, both dendritic inclusions and irregular solid particles are seen. At 15 min, there are no dendritic inclusions and only clusters of irregular solid particles exist. This finding implies that the large dendritic inclusions were floated out. Furthermore, clusters are generated by small particles attaching together during the RH degassing process. The same phenomena were also investigated in a small induction furnace experiment by Kunisada et al.[14]

1 min

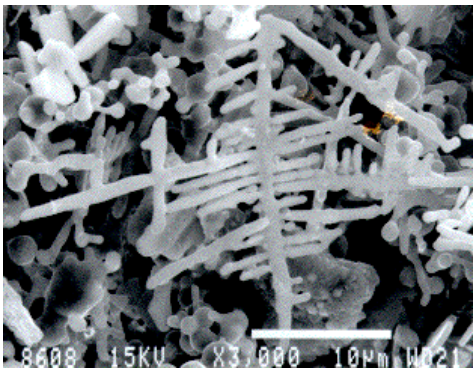

15 min

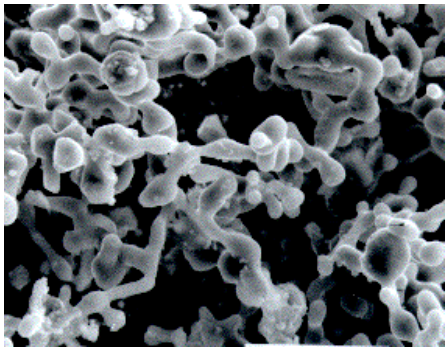

Photo.1 SEM image of inclusions at 1 min and 15 min after Aluminum addition.

4. CALCULATION RESULTS AND DISCUSSION.

4.1. Fluid Flow Simulation Results.

Fig.4 shows the velocity vectors calculated in the whole RH degasser using a 3-D single-model with 15000 nodes. The results are similar to that of previous research [15],[16],[17].

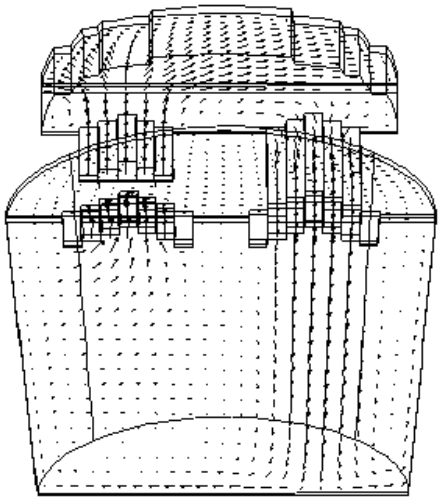

Fig.4 Calculated molten steel flow in RH degasser.

Fig.5 shows the trajectories of 2 typical 50 μm radius inclusions. Fig.6 shows the fraction of inclusions removed as a function of their size. Inclusions are removed when they contact the top surface of the ladle, and are based on 100 trajectories for each inclusion radius.

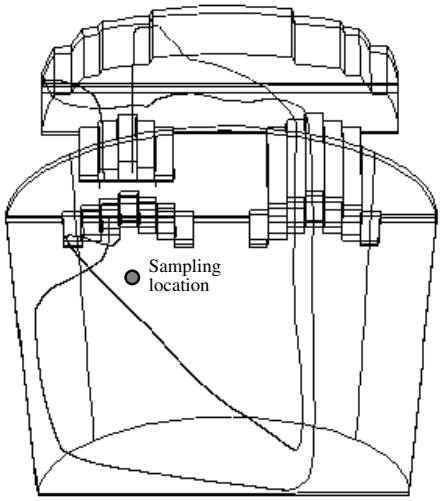

Fig.5 50 μm radius inclusion trajectories in RH degasser (ladle and vacuum vessel)

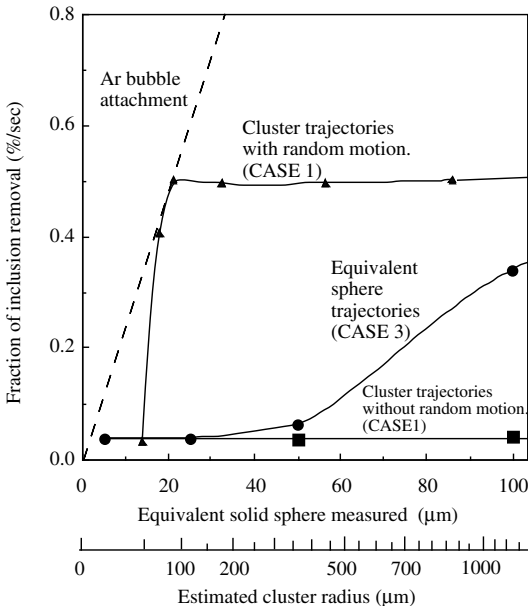

Fig.6 Comparison of inclusion removal fraction in the ladle for each size.

Fig.6 compares the removal rates between clusters (with density calculated in Eq.(15)) and equivalent solid spheres with Al_2O_3 density (CASE 3). The flotation removal rate of actual clusters is almost independent of their size and for the inclusion size distribution calculations that follow, the flotation velocity for CASE 3 is employed.

Fig.7 shows the trajectories of four 50 μm radius inclusions in the vacuum vessel. In the vacuum vessel, inclusions would be removed when they contact the top surface due to the surface tension effects. Nevertheless the contribution of entrapment to the top surface in the vacuum vessel was considered negligible relative to the effect of argon gas bubbles.

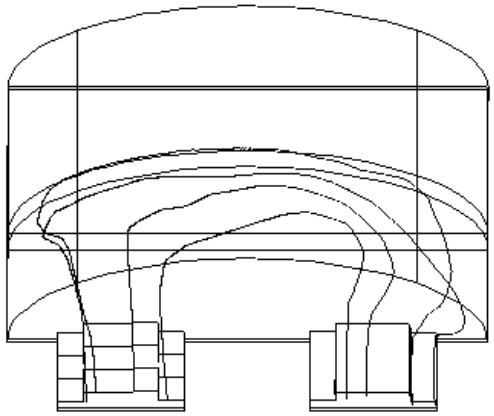

Fig.7 Trajectories of 50 μm radius inclusions in vacuum vessel.

Fig.8 shows the volume fractions of molten steel calculated with the 2-phase flow model. The top free surface above the up-leg (left) is raised about 0.15 m higher than that above the down leg. Argon is found to distribute throughout the up-leg and its contribution to inclusion removal from this part of the degasser was calculated. This numerical simulation predicts an argon volume fraction in this region of 0.2 within a volume of about 1.2 m^3. This volume represents only 3 % of the total RH degasser volume where steel can be.

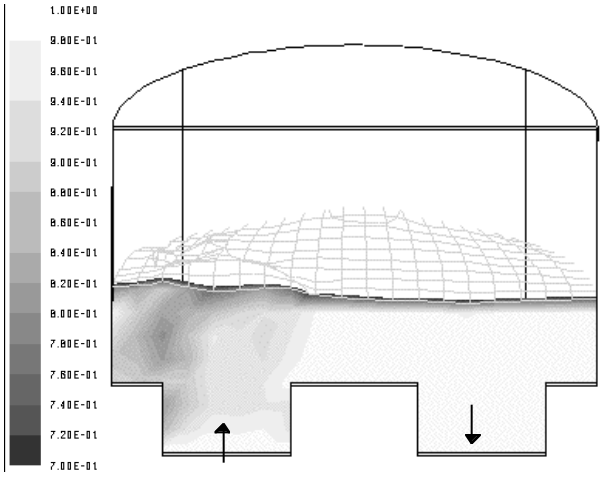

Fig.8 Calculation of steel-argon volume fractions and free surface (iso-volume-fraction of 0.5 steel). Black area has high argon fractions.

Fig.9 shows the calculated distribution of the turbulence dissipation rate in the vacuum vessel with the argon. Injecting argon gas increases the dissipation rate. The mean turbulence dissipation rate is 0.0068 m^2/s^3 for the ladle, 0.038 m^2/s^3 for the vacuum vessel and 0.01 m^2/s^3 for the whole vessel.

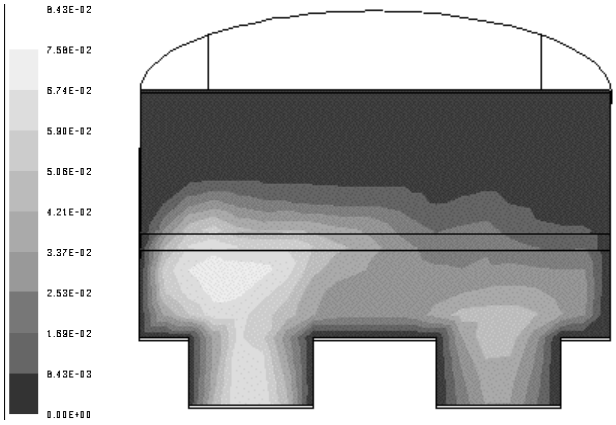

Fig.9 Distribution of turbulence dissipation rate.

4.2. Comparison of Calculated and Measured Inclusion Size Distribution.

In the experiments, aluminum is dissolved and Al_2O_3 particles are generated within 1 minute of adding aluminum to the top of the vacuum vessel. Collisions and flotation together determine the inclusion size distribution after that time. Thus, the inclusion size distribution at 1 min is employed for the initial size distribution. Subsequent inclusion size distributions are calculated by the model including distributions at 7 and 15 min, which are compared with measurements.

The evolution of inclusion size distributions was calculated with the models described in Section 2, with and without modifications for the effect of argon given in Sec 4.1. Fig.10 compares the calculated and measured inclusion size distributions without the argon effect. The calculations clearly do not coincide with the measurements. The excessive number of large inclusions predicted is responsible for the excessive removal of small inclusion sizes via collisions. This finding agrees with Higuchi et al.[18], who calculated inclusion size distribution during RH degassing and also suggested that if cluster density calculated by the volume fraction of Al_2O_3 in clusters is employed, the inclusion size distribution does not coincide with observations.

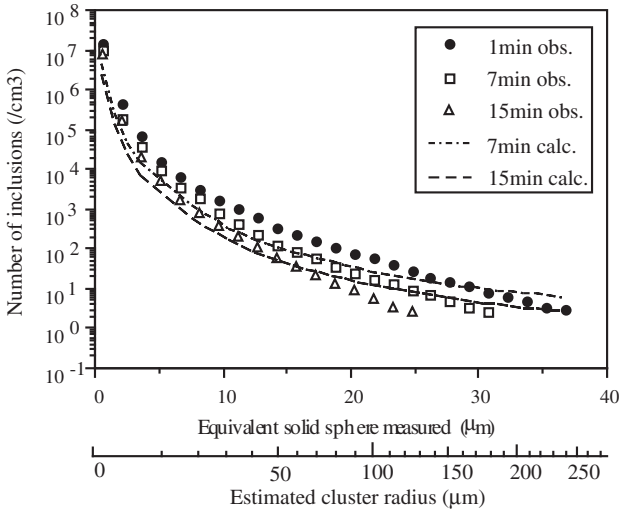

Fig.10 Comparison between measured inclusion size distribution in a RH degasser and that calculated by the model without random motion and without argon bubble effect.

Fig.11 shows the results calculated with the turbulent random motion effect and no argon bubble effect. Even with the large flotation velocity, the removal rate of large inclusions is still greatly underpredicted.

Fig.12 compares the calculated and measured inclusion size distributions with the argon effect. This effect was incorporated using the turbulence dissipation rate 0.01 m^2/s^3 with 3 % chance of inclusions being present in the 1.2 m^3 volume containing 20% argon based on calculations by 3-D flow model.

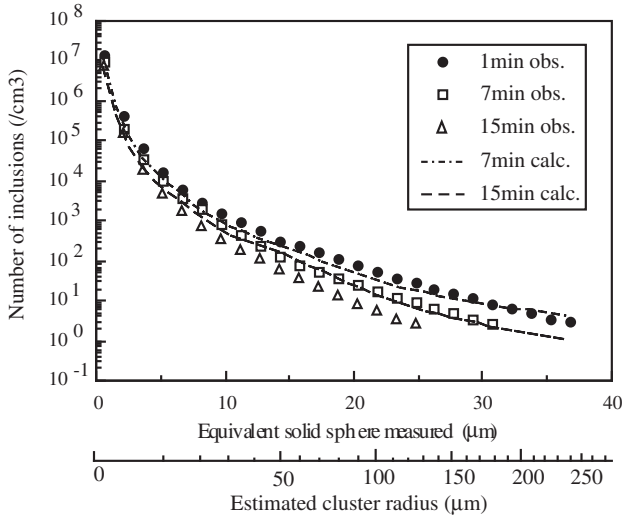

Fig.11 Comparison between measured inclusion size distribution in a RH degasser and that calculated by the model with turbulent random motion but no argon bubble effect.

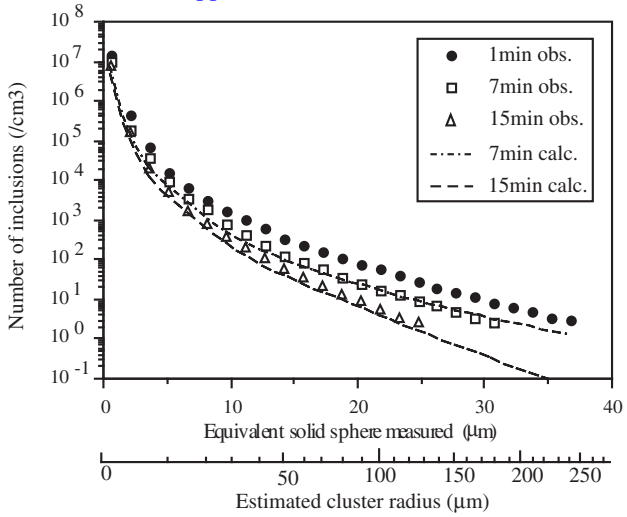

Fig.12 Comparison between measured inclusion size distribution in a RH degasser and that calculated by the model with argon bubble effect.

These results are seen to coincide. This suggests that large inclusions are removed by their entrapment to argon bubbles.

This work provides evidence that argon gas injected into the molten steel distributes argon bubbles above the up-leg, which attach inclusions and promote inclusion removal. Fig.13 shows the change of the inclusion size distribution calculated without inclusion collision. The number of inclusions smaller than 5 μm does not change with time. Thus, the number of inclusions less than 10 μm (cluster radius 25 μm) is overpredicted (does not decrease as measured). Correspondingly, the number of inclusions larger than 15 μm is smaller than observed. This shows that inclusion collision is also very important to inclusion redistribution and removal.

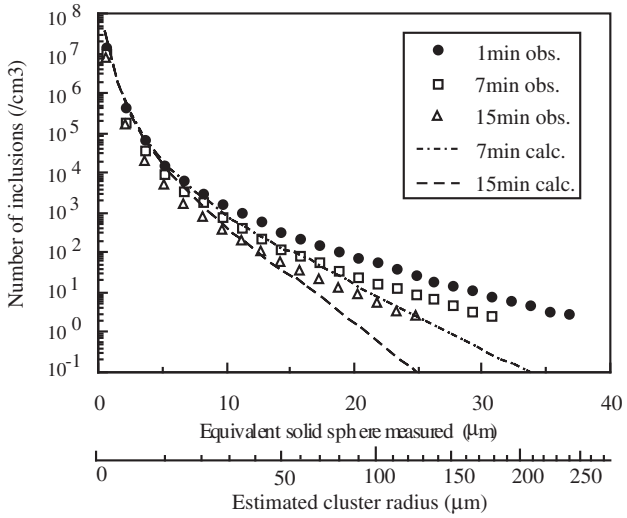

Fig.13 Comparison between measured inclusion size distribution in a RH degasser and that calculated by the model without inclusion collision and with argon bubble effect.

4.3. Mechanism of Inclusion Removal.

Fig.14 shows the oxygen contents calculated for each size range based on measured inclusion size distributions. Each radius represents the average inclusion size for the size interval, which was incremented by 1.5 µm. We notice that more than 50% of the oxygen content comes from inclusions with radius less than 5 µm. This result explains why the turbulence dissipation rate, which affects inclusions smaller than 5 µm in radius, is very influential on the total oxygen content.

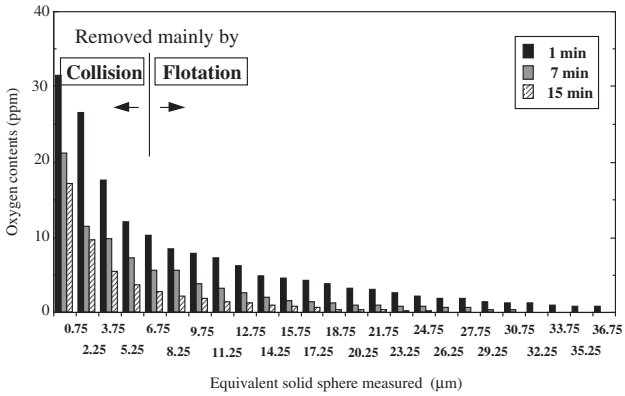

Fig.14 Oxygen content of Al_2O_3 inclusions for each radius with 1.5 µm range per bin in RH degasser.

Inclusion coagulation due to collisions are mainly responsible for the decrease in inclusion population for the smaller particles (<5 µm radius). The number of larger inclusions is controlled by a balance between inclusion coagulation, which generates large inclusion clusters, and inclusion removal via rapid flotation due to bubble attachment and turbulent random motion near the surface.

4.4. Effect of Turbulence Dissipation Rate.

Fig.15 shows calculated and observed total Al_2O_3 contents in the ladle during RH degassing. These results were obtained by integrating the previous inclusion size distributions. The measured results agree with the calculations with the standard turbulence dissipation rate of 0.01 m^2/s^3. The Al_2O_3 content with dissipation rate of 0.05 m^2/s^3 levels off after 600 sec.

Fig.16 shows the calculated inclusion size distribution for each turbulence dissipation rate at 15 min after aluminum addition. The number of 35 µm radius inclusions calculated with the lowest dissipation rate of 0.001 m^2/s^3 is smaller due to the smaller collision rate.

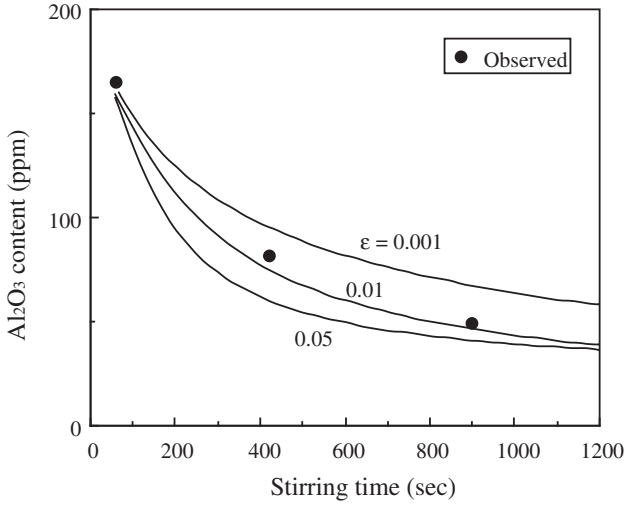

Fig.15 Change of calculated and observed Al_2O_3 content.

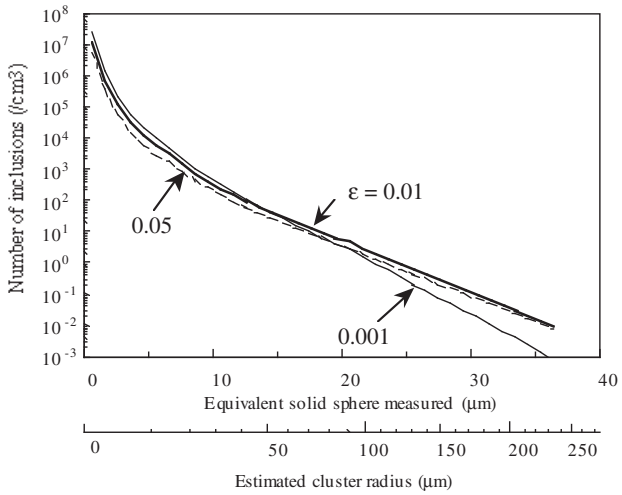

Fig.16 Comparison of inclusion size distribution calculated with the different turbulence dissipation rate.

4.5. Implications.

Increased argon flow appears to enhance productivity in inclusion removal in several ways
-attaches to large inclusions to remove them directly.
-increases turbulence
Little benefit is obtained by increased the stirring time longer than 900 sec (mean residence time > 12) in removing inclusions from the RH degasser. Thus, current plant practice was not changed. Further significant decreases in inclusions would require higher dissipation rates for coagulation and/or larger argon gas flow rate.
Other processes which involve argon stirring such as LF (ladle furnace) and VOD (vacuum oxygen decarburization) likely also benefit by removing inclusions due to argon bubble attachment.

5. CONCLUSIONS.

A model of inclusion size distribution during RH degassing has been developed and validated with measurement. The following results were obtained.

1) The RH degasser is capable of lowering Al_2O_3 content from more than 150 ppm to less than 50 ppm in 12 mean residence times.
2) 1 min after aluminum addition, large dendritic inclusions were found. After 15 min of stirring in the RH degasser, the dendritic inclusions disappear and large clusters were found. Clearly the dendritic inclusions are able to float out, while smaller inclusions coagulate.
3) The calculated inclusion size distribution only agrees with observed one when collision, flotation and attachment to argon bubbles are all considered.
4) Random turbulence motion near the surface is effective at removing large inclusions.
5) Argon gas bubbles concentrate above the up-leg, where they attach with inclusions. Inclusion flotation by attachment to argon bubbles decreases mainly the number of large inclusions.
6) Increasing the turbulence dissipation rate is effective for deoxidation since the number of small inclusions, such as 5 μm in radius, are controlled by inclusion collision and most of the oxygen content comes from the small inclusions. This can be done by increasing the argon flow during degassing.
7) A low dissipation rate and/or large amount of argon gas may be effective in reducing the number of large inclusions (>20 μm) even though the total oxygen content increases.

ACKNOWLEDGMENT

The authors wish to thank Dr Fujii, Dr Sorimachi and Dr Bessho of Kawasaki steel for useful advice. Thanks are also due to the National Center for Supercomputing Applications at University of Illinois for computer time and use of the FLUENT code.

REFERENCES

1)U.Lindborg and K.Torssell, Trans.Metall.Soc.AIME, Vol.242, 1968, pp.94-102.
2)K.Nakanishi and J.Szekely, Trans.ISIJ, Vol.15 1975, pp.522-530.
3) P.G.Saffman and J.S. Turner , J. Fluid Mech.,Vol.1, 1956, pp.16-30.
4)K.Higashitani, K.Yamauchi, Y.Matsuno and G.Hosokawa, J.Chem.Eng. Jpn, Vol.l16, 1983, pp.299-304.
5)R.C.Sussman, M.T.Burns, X.Huang and B.G.Thomas, 10th PTD Conf. Proceedings, 1992, pp.291-299.
6)L.Wang, H.G.Lee and P.Hayes, ISIJ Int., Vol.36, 1996, 1, pp.7-16.
7) H.Yasuhara, Simura and S.Nabeshima, CAMP-ISIJ, ,1996, 5, pp.785.
8)Fluent user's guide Vol.1-3, Fluent Inc., Lebanon, NH 1995
9)For example, F.M.White, Viscous fluid flow, MacGraw-Gill Inc., 1991, pp.176
10)Tadaki and S.Maeda, Kagaku-kougaku, Vol.25, 1961, pp.254-262.
11)K.Tozawa, Y.Kato and T.Nakanishi, CAMP-ISIJ, 1994, 7, pp.276.
12)K.Asano and T.Nakano, Tetsu-to-hagane, Vol.57, 1971, pp.1943-1951.
13)S.Taniguchi and A.Kikuchi, Tetsu-to-hagane, Vol.78, 1992, pp.527-535.
14)Kunisada and H.Iwai , CAMP-ISIJ, 1991, 4, pp.1234.
15)R.Tsujino, J.Nakashima, M.Hirai and I.Sawada, ISIJ Int., Vol.29, 1989, 7, pp.589-595.
16)Y.Kato, H.Nakato, T.Fujii, S.Ohmiya and S.Takatori, Tetsu-to-hagane, 77, 1991, 10, pp.1664-1671.
17)M.Szatkowski and M.C.Tsai, I&SM, April 1991, pp.65-71.
18) Y.Higuchi, Y.Shirota, T.Obana and H.Ikeda, CAMP-ISIJ., 4, 1991, pp.266.

APPENDIX

Saffman's theory[3] has the following important assumptions.

(a)Particles have spherical shape.

(b)Particle radius is smaller than turbulence eddies.

Concerning (b), the minimum diameter of the turbulence eddy, λ, was estimated by Kolmogolov's dimensional analysis.

$$\lambda = \left(\frac{\nu^3}{\varepsilon}\right)^{0.25} \qquad \text{(a1)}$$

Where, ν : kinematic viscosity, ε : dissipation rate of turbulence energy.

Using Eq.(a1), the diameter, λ, is estimated to be about 90 μm when ε is 0.01 m^2/s^3.

Thus, Saffman's model[3] can be applied when the inclusions are smaller than 90 μm. It is not clear how much smaller inclusions can be applied in Saffman's model. However, the coefficient of collision, α introduced by Higashitani[4], becomes small when the radius is large. Also, the number of large inclusions is small. The collision rate, W_t, is the product of α and the number of inclusions so that W_t for inclusions of more than 10 μm radius is very small and negligible. Therefore, the turbulence collision rate using Higashitani's model should be reasonable for the whole range of inclusion radii in this work.